JET-P(95)12

More on Core-localized Toroidal Alfvén Eigenmodes

H L Berk[1], D Borba, J Candy, G T A Huysmans,
S Sharapov, J W Van Dam[1].

JET Joint Undertaking, Abingdon, Oxfordshire, OX14 3EA, UK.
[1] Institute for Fusion Studies, The University of Texas at Austin,
Austin, Texas, 78712, USA.

Preprint of a paper to be submitted for publication in
Physics of Plasmas

April 1995

Abstract

A novel type of ideal toroidal Alfvén eigenmode, localized in the low-shear core region of a tokamak plasma, is shown to exist, whose frequency is near the upper continuum of the toroidal Alfvén gap. This mode converts to a kinetic-type toroidal Alfvén eigenmode above a critical threshold that depends on aspect ratio, pressure gradient, and shear. Opposite to the usual ideal toroidal Alfvén eigenmode, this new mode is peaked in amplitude on the small-major-radius side of the plasma.

I. INTRODUCTION

A surprising recent result from NOVA code simulations[1] of a certain D-T discharge in the TFTR tokamak[2] was the finding of a core-localized toroidal Alfvén eigenmode (TAE), at a plasma pressure gradient value considerably higher than would have been expected theoretically.[3-5] An explanation for this result has been given by Fu[6] from an analytic solution of the finite-frequency ballooning equation with finite aspect ratio terms carefully included. The aim of the present paper is to point out that the finite aspect ratio terms that Fu considered also lead to the existence of a second core-localized ideal TAE within the Alfvén continuum gap. This latter mode had, in fact, previously been noticed in results from numerical calculations.[7] Furthermore, we show how both of these core-localized modes convert to kinetic toroidal Alfvén eigenmodes (KTAE)[8-10] when the parameter values for shear, pressure gradient, and aspect ratio are varied.

II. ANALYSIS

In the reduced MHD description, the linearized eigenmode equation for the perturbation amplitude $\Phi = \exp(-i\omega t + in\phi) \sum_m \phi_m(r) e^{-im\theta}$ is, in the limit of large toroidal mode number ($n \gg 1$), given by

$$\left[\mathbf{B}\cdot\boldsymbol{\nabla}\left(\frac{1}{B}\nabla_\perp^2\frac{1}{B}\mathbf{B}\cdot\boldsymbol{\nabla}\right)+\boldsymbol{\nabla}\cdot\left(\frac{\omega^2}{v_A^2}\boldsymbol{\nabla}_\perp\right)+\frac{8\pi}{B^2}(\mathbf{B}\times\boldsymbol{\kappa})\cdot\boldsymbol{\nabla}_\perp\left(\frac{1}{B^2}\mathbf{B}\times\boldsymbol{\nabla}p\right)\cdot\boldsymbol{\nabla}_\perp\right]\Phi=0. \tag{1}$$

Here, ω is the eigenvalue, v_A the Alfvén speed, $\boldsymbol{\kappa}$ the magnetic field line curvature ($|\boldsymbol{\kappa}| = 1/R$, with R the major radius), p the plasma pressure, and $\mathbf{B}$ the equilibrium magnetic field. To analyze Eq. (1), we assume small inverse aspect ratio ($\epsilon \equiv r/R \ll 1$), so that only two poloidal harmonics ϕ_m and ϕ_{m+1} are excited near the shear Alfvén gap at $r = r_m$, with r_m such that $q(r_m) = (m + 1/2)/n$, where q is the safety factor. We focus attention on the core

region where the shear $s = d(\ln q)/d(\ln r)$ is low. In the $s \ll 1$ limit (more precisely, when the condition $n\epsilon e^{-1/s} \ll 1$ is satisfied[11]), the mode amplitude is localized in the vicinity of this gap. Then, in a straightforward procedure,[12] Eq. (1) can be rewritten as the following set of coupled equations:

$$\frac{d}{dy}\left[(y+1/2)^2-\Omega^2\right]\frac{d\phi_m}{dy}-\frac{1}{s^2}\left[(y+1/2)^2-\Omega^2\right]\phi_m$$
$$-\left[\Omega^2(2\epsilon+\Delta')+\frac{\Delta'}{4}\right]\frac{d^2\phi_{m+1}}{dy^2}+\frac{1}{s^2}\left[\Omega^2(\epsilon-\Delta')-\frac{1}{4}(\epsilon+\Delta')+\alpha/2\right]\phi_{m+1}=0, \quad (2)$$

$$\frac{d}{dy}\left[(y-1/2)^2-\Omega^2\right]\frac{d\phi_{m+1}}{dy}-\frac{1}{s^2}\left[(y-1/2)^2-\Omega^2\right]\phi_{m+1}$$
$$-\left[\Omega^2(2\epsilon+\Delta')+\frac{\Delta'}{4}\right]\frac{d^2\phi_m}{dy^2}+\frac{1}{s^2}\left[\Omega^2(\epsilon-\Delta')-\frac{1}{4}(\epsilon+\Delta')+\alpha/2\right]\phi_m=0. \quad (3)$$

Here, $\alpha = -8\pi Rq^2B^{-2}(dp/dr)$ is the normalized pressure gradient; Δ' is the radial derivative of the Shafranov shift; $\Omega = \omega/2\omega_0$ is the normalized frequency, with $\omega_0 = v_A(r_m)/2q(r_m)R_0$; and $y = n[q - q(r_m)]$ is the radial coordinate.

We will look for the core-localized modes near the tips of the continuum at the two ends of the gap. Introduce $g = (\omega^2 - \omega_0^2)/\hat{\epsilon}\omega_0^2$, the normalized shift of the frequency from the Alfvén gap central frequency ω_0, where $\hat{\epsilon} = 2(\epsilon + \Delta')$ is the toroidicity coupling coefficient; then $g = +1$ and -1 correspond, respectively, to the upper and lower ends of the gap. We can treat both ends simultaneously by writing $g = g_0(1 - g_1)$, with $g_0 = \pm 1$, where we seek solutions with $g_1 \ll 1$. For these frequencies of interest, it is particularly useful to define the sum and difference combinations $\psi_1 = \phi_m - g_0\phi_{m+1}$ and $\psi_2 = g_0\phi_m + \phi_{m+1}$. The coupled equations for these new field amplitudes, with scaled radial variable $z = y/s$, are

$$\left(\frac{d}{dz}z\frac{d}{dz}-z\right)\psi_1+s\left[g_0z\left(\frac{d}{dz}z\frac{d}{dz}-z\right)-\frac{\hat{\epsilon}}{2s^2}\frac{d^2}{dz^2}+g_0z\frac{d}{dz}+\frac{\epsilon+\alpha}{2s^2}\right]\psi_2=0, \quad (4)$$

$$\left(\frac{d}{dz}z\frac{d}{dz}-z\right)\psi_2+s\left[g_0z\left(\frac{d}{dz}z\frac{d}{dz}-z\right)-\frac{\hat{\epsilon}g_1}{4s^2}\frac{d^2}{dz^2}+g_0z\frac{d}{dz}+\frac{\epsilon-\alpha}{2s^2}\right]\psi_1=0, \quad (5)$$

with $\delta = \epsilon + 2\Delta'$. The form of Eqs. (4) and (5) has the advantage that it exhibits an obvious ordering when $\hat{\epsilon}$ and α are taken to be $\mathcal{O}(s^2) \ll 1$; it will be seen *a posteriori* that g_1 is also $\mathcal{O}(s^2)$.

With this ordering, the solution of Eqs. (4) and (5) becomes a boundary-layer problem. In the outer region (where $z \approx 1$), to lowest order in the smallness parameter s the solutions well-behaved at $|z| \to \infty$ are

$$\psi_1(z) = -\hat{C}_1 K_0(|z|) \qquad \text{and} \qquad \psi_2(z) = -\hat{C}_2 K_0(|z|) \tag{6}$$

with $\hat{C}_1$ and $\hat{C}_2$ constants and K_0 the Macdonald function. These lowest-order solutions need to be matched to the solutions that are valid in the inner layer region, where $z \approx \hat{\epsilon} g_1^{1/2}/s = \mathcal{O}(s^2) \ll 1$.

In the inner region, since the solutions are peaked, only the high-order radial derivative terms of Eqs. (4) and (5) contribute. Their first integrals can be written, in terms of the new variable $x = 4sz/\hat{\epsilon} g_1^{1/2}$, as

$$-\frac{g_0 \lambda^2}{g_1^2} \frac{d^2\psi_1'}{dx^2} + \frac{x}{g_1^{1/2}} \psi_2' + \psi_1' = \frac{1}{g_1^{1/2}} \hat{C}_2, \tag{7}$$

$$x\psi_1' - \frac{2}{g_1^{1/2}} \psi_2' = \hat{C}_1, \tag{8}$$

where a prime denotes a derivative with respect to x, and $\hat{C}_1$ and $\hat{C}_2$ are the same integration constants as in Eq. (6). In the inner region ($x \approx 1$) we have added nonideal effects[8-10] due to finite ion Larmor radius and parallel electron conductivity, represented by the first term in Eq. (7). Here, $\lambda^2 = 8n^2 s^2 q^2 (r_{Le}^2 + \frac{3}{4} r_{Li}^2)/\hat{\epsilon}^3 r^2$ plus a small collisional correction such that $\mathrm{Im}\, \lambda^2 \leq 0$, with r_{Li} the ion Larmor radius and $r_{Le} \cong r_{Li} (T_e/T_i)^{1/2}$. Observe that $\psi_2'/\psi_1' = \mathcal{O}(s) \ll 1$ holds in the inner region; this is what motivated the choice of the particular forms for ψ_1 and ψ_2. Combining Eqs. (7) and (8) leads to the single equation

$$-\frac{g_0 \lambda^2}{g_1^2} \frac{d^2\psi_1'}{dx^2} + \left(\frac{1}{2} x^2 + 1\right) \psi_1' = \frac{1}{g_1^{1/2}} \hat{C}_2 + x\hat{C}_1. \tag{9}$$

whose solution, obtained by means of a Fourier transform technique,[9,10] then yields the following "jumps" in ψ_1 and ψ_2:

$$\Delta\psi_1 = \frac{\pi \hat{C}_2}{\lambda^{1/2}(2g_0)^{1/4}} \frac{\Gamma\left(\frac{1}{4} + \frac{\hat{\omega}}{g_0^{1/2}}\right)}{\Gamma\left(\frac{3}{4} + \frac{\hat{\omega}}{g_0^{1/2}}\right)}, \tag{10}$$

$$\Delta\psi_2 = -\lambda^{1/2}(2g_0)^{1/4}\pi \hat{C}_1 \frac{\Gamma\left(\frac{3}{4} + \frac{\hat{\omega}}{g_0^{1/2}}\right)}{\Gamma\left(\frac{1}{4} + \frac{\hat{\omega}}{g_0^{1/2}}\right)}. \tag{11}$$

with $\hat{\omega} = g_1/2^{3/2}\lambda$.

III. EVALUATION OF CORE-LOCALIZED EIGENMODES

The jumps across the inner layer must be matched to the corresponding jumps found from the outer region, to obtain a dispersion relation. The matching procedure separates into the two cases of $\hat{C}_2 = 0$ and $\hat{C}_1 = 0$, related to the parity of the inner layer KTAE solution (ψ_1 even and odd, respectively). The former is the more interesting case because it has both ideal and nonideal solutions, continuously connected, and its KTAE modes are known[13] to have a lower instability threshold.

Case 1: $\hat{C}_2 = 0$

In this case the matching is straightforward, with the ordering $\psi_2/\psi_1 = \mathcal{O}(s) \ll 1$. To lowest order in s, the outer solution is $\psi_1 = -\hat{C}_1 K_0(|z|)$, which reproduces the logarithmic Alfvén singularity near the gap and matches onto the condition $\Delta\psi_1 = 0$. The jump $\Delta\psi_2$ in the outer region is next order in s and can be derived from the regular Green's function solution of Eq. (4) with the use of the lowest-order form for ψ_1:

$$\Delta\psi_2 = -2s\hat{C}_1 \int_0^\infty dz\, K_0(z) \left[\frac{\delta - \alpha}{2s^2} + g_0 z \frac{d}{dz}\right] K_0(z) = \frac{\pi^2 s}{4}\left(g_0 - \frac{\delta - \alpha}{s^2}\right). \tag{12}$$

Equating this result to Eq. (11) gives a general dispersion relation, which we now examine specifically for the two ends of the frequency gap.

(a) Upper end of the gap ($g_0 = 1$):

The dispersion relation is given by

$$\frac{\Gamma\left(\frac{3}{4}+\hat{\omega}\right)}{\Gamma\left(\frac{1}{4}+\hat{\omega}\right)} = \frac{\pi s}{2^{9/4}\lambda^{1/2}}\left(-1+\frac{\delta-\alpha}{s^2}\right) \equiv a. \tag{13}$$

We can gain graphical insight into the roots of Eq. (13) by plotting its left-hand side as a function of $\hat{\omega}$, as shown in Fig. 1. The roots are located where this function is equal to a, where a may be either positive or negative, depending upon parameters.

KTAE roots (i.e., $\hat{\omega} < 0$, corresponding to frequencies lying in the ideal continuum) occur just below $\hat{\omega} = -\frac{1}{4} - p$ when $a \ll -1$; near $\hat{\omega} = -\frac{1}{2} - p$ when $|a| \ll 1$; and just above $\hat{\omega} = -\frac{3}{4} - p$ when $a \gg 1$, with $p = 0, 1, 2 \ldots$.

One exception occurs when $a > \pi^{1/2}/4$, in which case a positive root (lying in the ideal gap) can arise. When nonideal effects are negligible ($a \gg 1$), this root is given by $\hat{\omega} \approx a^2$, and it can be obtained directly from the ideal TAE equations. Figure 2 shows a plot of this root as a function of a, compared with the approximate expressions $\hat{\omega} \cong a^2$ when $a \ll -1$, $\hat{\omega} \cong -1/4 + a/\pi$ when $|a| \ll 1$, and $\hat{\omega} \cong -3/4 - 1/(2a + \pi)$ when $a \gg 1$.

Note that all the roots are undamped, to the extent that λ is real; tunneling, collisional dissipation, and ion Landau damping, if taken into account, can give λ a small imaginary part and cause the roots to be slightly damped.[9,10]

(a) Lower end of the gap ($g_0 = -1$):

The dispersion relation, given by

$$\frac{\Gamma\left(\frac{3}{4}-i\hat{\omega}\right)}{\Gamma\left(\frac{1}{4}-i\hat{\omega}\right)} = \frac{\pi s}{2^{9/4}\lambda^{1/2}}\left(1+\frac{\delta-\alpha}{s^2}\right)e^{-i\pi/4} \equiv be^{-i\pi/4} \tag{14}$$

is intrinsically complex. In Figs. 3(a) and (b) we show, respectively, the real and imaginary parts of the principal root as a function of b, together with analytic approximations for various values of b. When $b \gg 1$, the principal root goes over to an ideal root, approximately given by $\widehat{\omega} = b^2[1 - 2i\exp(-2\pi b^2)]$; note that radiation damping for this root is small, even for $b \approx 1$, due to the large exponential coefficient. In two other asymptotic limits, the principal root is seen to be a KTAE mode with appreciable damping, being approximately given by $\widehat{\omega} = -i\pi/4 + b\pi^{-1/2}\exp(i\pi/4)$ when $|b| \ll 1$ and $\widehat{\omega} = -3i\pi/4 - \exp(-i\pi/4)/2|b|\pi^{1/2}$ when $b \ll -1$.

In the ideal limit ($\lambda \to 0$), the condition for the core-localized mode at the *lower* end of the gap to exist is $\alpha < \delta + s^2$, which was derived by Fu.[6] For this mode, the critical beta value above which the mode shifts into the ideal continuum is increased by finite aspect ratio effects, which is consistent with the NOVA simulation results.[1] The corresponding condition for the ideal core-localized mode at the upper end of the gap is $\alpha < -s^2 + \delta$, which shows that finite aspect ratio effects are essential for its existence. The lower core-localized mode of Fu[6] is the finite-ϵ, finite-β generalization of the usual ideal TAE at low shear, whereas the upper mode gives a new ideal TAE. Both modes take into account finite-ϵ effects not only in the inner region (as with earlier TAE theories), but now also in the outer region. As the plasma beta value increases, the upper core-localized mode enters the continuum first. We have here demonstrated how both upper and lower core-localized modes are converted into KTAE modes.

Case 2: $\widehat{C}_1 = 0$

As before, we match inner region and outer region jumps. In this case, however, the evaluation of the outer jump requires that an apparent divergence be removed. The lowest-order outer solution is $\psi_2 = -\widehat{C}_2 K_0(|z|)$. Using the symmetry properties of ψ_2 and the regular Green's function solution of Eq. (4) for ψ_1, we can write the jump in ψ_1 across the

origin nearly exactly as

$$\Delta\psi_1 = 2s\int_0^\infty dz\, K_0(z)\left[-\frac{\widehat{\epsilon}}{2s^2}\frac{d^2\psi_2}{dz^2} + \frac{\epsilon+\alpha}{2s^2}\psi_2 + g_0 z\frac{d\psi_2}{dz}\right]. \tag{15}$$

For evaluating the last two terms in this integral, the K_0 solution for ψ_2 may be employed, since convergence near the origin is sufficiently rapid. For the first term we need to be more careful, by including the behavior of ψ_2 when $z \lesssim \widehat{\epsilon} g_1^{1/2}/s \approx s^2$. Let $\psi_2^{\rm in}$ denote the exact inner-layer solution, from Eq. (8). Since this has even parity in z and is nonsingular, we can integrate by parts and write the first term of the integral in Eq. (15) — call it $\Delta\psi_1^{(1)}$ — as follows:

$$\Delta\psi_1^{(1)} = \frac{\widehat{\epsilon}}{s}\int_0^\infty dz\,\frac{dK_0}{dz}\frac{d\psi_2}{dz}. \tag{16}$$

Let L be a distance between the inner region and outer region scale lengths: $\widehat{\epsilon} g_1^{1/2}/s \ll L \ll 1$. For $z < L$, we can approximate $dK_0(z)/dz \cong -1/z$ and use $d\psi_2/dz \cong d\psi_2^{\rm in}/dz$. Likewise, for $z > L$, we can use $d\psi_2/dz \cong -\widehat{C}_2 dK_0/dz$ and $d\psi_2^{\rm in}/dz \cong \widehat{C}_2/z$. Then $\Delta\psi_1^{(1)}$ can be written as

$$\Delta\psi_1^{(1)} = -\frac{\widehat{\epsilon}}{s}\int_0^\infty \frac{dz}{z}\frac{d\psi_2^{\rm in}}{dz} + \frac{\widehat{\epsilon}}{s}\widehat{C}_2\int_0^\infty dz\left[\frac{1}{z^2} - \left(\frac{dK_0}{dz}\right)^2\right]. \tag{17}$$

The first term in Eq. (17) is just the jump that arises from the inner solution, as can be seen from Eq. (8), and has been already evaluated in Eq. (10). To avoid double counting, we ignore this term. The second term in Eq. (17) can be exactly integrated, yielding the total jump in the outer region,

$$\Delta\psi_1 = \frac{\pi^2 s}{4}\left(\frac{\delta-\alpha}{s^2} + g_0\right)\widehat{C}_2. \tag{18}$$

which is to be equated to Eq. (10).

Again, first consider the upper end of the gap ($g_0 = 1$). The dispersion relation is

$$\frac{\Gamma(\frac{1}{4}+\widehat{\omega})}{\Gamma(\frac{3}{4}+\widehat{\omega})} = \frac{\pi s\lambda^{1/2}}{2^{7/4}}\left(1 + \frac{\delta-\alpha}{s^2}\right) \equiv c. \tag{19}$$

The right-hand side, c, is proportional to $s\lambda^{1/2}$ and hence always small compared to unity, so KTAE roots occur near $\widehat{\omega} = -3/4 - p$, with p a positive integer. For example, the frequency

shift for the smallest root ($p = 0$) can be calculated, which gives $\hat{\omega} = -3/4 - c/2\pi^{1/2}$; this result was previously obtained without finite beta and aspect ratio effects.[13] (Another root from Eq. (19), $\hat{\omega} = 1/c^2$, which gives $g_1 \approx 1/s$, is spurious since our analysis requires $|g_1| \ll 1$.) When $|c| \ll 1$ and also $|a| \ll 1$ [cf. Eq. (13)], the KTAE roots here are paired with those from the $\hat{C}_2 = 0$ case at the upper end of the gap, with only a fine frequency splitting between them.[10,13]

At the lower end of the gap ($g_0 = -1$), the dispersion relation has the same form as in Eq. (19) with the substitutions $\hat{\omega} \to -i\hat{\omega}$ and $+1 \to -1$ on the right-hand side. This has only damped solutions, given by $\hat{\omega} = -i(3/4 + p)$, with p a positive integer.

There are no ideal roots in the $\hat{C}_1 = 0$ case.

IV. COMPARISON WITH NUMERICAL SOLUTIONS

It should be pointed out that the basic equations, Eqs. (2) and (3), are derived from a model equilibrium that is accurate only to first order in ϵ. Consequently, the analytical theory in the present paper is valid only in the limit $\hat{\epsilon} \ll s$. This ordering, however, may break down for realistic tokamak equilibria. Then the separation into inner and outer regions cannot be used, even for the ideal core-localized TAE. Nevertheless, direct numerical integration of Eqs. (2) and (3) shows that two core-localized TAE modes can still exist when the small-$\hat{\epsilon}$ ordering is not satisfied.

Another such example, calculated with the CASTOR code[7] for a realistic equilibrium, for the case $\hat{\epsilon} \geq s$ and with toroidal mode number $n = 5$, is shown in Figs. 4-6. These results correspond to the particular TFTR equilibrium (shot #76770) mentioned earlier,[1,2] with pressure profile $p(\psi) = p(0)(1 - \psi)(1 - 1.288\psi + 0.943\psi^2)$, density profile $\rho(\psi) = \rho(0)(1 - 0.99\psi)(1 + 0.5\psi)$ and the current profile $j(\psi) = j(0)(1 - 1.515\psi + 0.615\psi^3)$, where $\psi = \psi_p/\psi_{\mathrm{edge}}$ is the normalized poloidal flux. Both of the core-localized modes are associated

with the same gap near the center of the plasma, with $\epsilon = 0.035$ and $s = 0.048$. Figure 4 shows the low-end mode, and Fig. 5 the high-end mode, both dominantly consisting of the $m = 4$ and $m = 5$ poloidal harmonics. Note that these modes have opposite polarizations, i.e., $\mathrm{sgn}(\phi_{m=4}/\phi_{m=5}) = -g_0$, and eigenfrequencies located near the corresponding edges of the gap, in qualitative agreement with the theoretical analysis, even though the $\hat{\epsilon} \ll s$ ordering is not satisfied.

Figure 6 shows the CASTOR code results for the mode eigenfrequencies as the central plasma pressure $p(0)$ is increased, together with the results obtained from direct integration of the model equations, Eqs. (2) and (3). For the model equations, parameters were chosen that map the model Alfvén continua onto the CASTOR continua and yield the same values for the quantities s, ϵ, and Δ' as $p(0)$ varies. Both sets of numerical results show that the upper and lower core-localized modes approach the Alfvén continuum with increasing pressure; this behavior also agrees with the analytic prediction. In the CASTOR results, the upper TAE reaches the continuum at $\alpha^{+}_{\mathrm{crit}} \cong 0.131$ (with $\epsilon = 0.035$, $\Delta' = 0.045$, and $s = 0.048$), before the lower TAE does at $\alpha^{-}_{\mathrm{crit}} \cong 0.152$ (with $\epsilon = 0.034$, $\Delta' = 0.050$, and $s = 0.048$), in agreement with the corresponding analytic thresholds $\alpha^{\pm} = \delta \mp s^2$. The results obtained from integrating the model equations also exhibit the same behavior and agreement at threshold. Below threshold, the frequency shift from the continuum as calculated from analytic theory is somewhat different from that obtained from the CASTOR code; we suspect that the high-n approximation in the analytic theory is a source of this disparity.

In Fu's analysis[6] of finite aspect ratio effects (also with the ordering $\hat{\epsilon} \ll s$), he used a ballooning mode type of treatment, which is valid[11] when $n\epsilon e^{-1/s} \gg 1$; this would then lead to replicating local mode structures at each location where $q(r) = (m + 1/2)/n$, for many m values. However, when the opposite inequality $n\epsilon e^{-1/s} \ll 1$ is satisfied, as in our treatment, then the eigenmode will truly have a single localized structure due to the m and $m + 1$ poloidal harmonics near $q(r) = (m + 1/2)/n$. Nevertheless, the eigenvalues obtained with a

ballooning theory will differ only slightly, because the mode overlap between successive gaps is exponentially small in the low-shear limit.

We again note that the lower frequency core-localized mode, found by Fu,[6] tends to be strongly damped by radiation damping as its frequency approaches the continuum, whereas the new core-localized mode at the high end of the gap has negligible radiation damping. Hence this new mode may be experimentally observable at moderate beta values when the other mode is suppressed by radiation damping.

Finally, we note that there may be a relatively straightforward experimental method for distinguishing the upper core-localized mode from the lower one, if appropriate core plasma diagnostics are used. Since their polarizations are determined (in Case 1) by $\phi_m + g_0\phi_{m+1} \cong 0$, the time-averaged power signal corresponding to the lower core-localized mode will peak on the outboard tokamak midplane, being proportional to $\cos^2(\theta/2)$, whereas that for the upper core-localized mode, proportional to $\sin^2(\theta/2)$, will be peaked on the inboard side of the plasma.

We acknowledge our gratitude to Dr. G. Y. Fu for showing us his results prior to publication and checking the comparison with the NOVA-K results, and to Dr. B. N. Breizman for pointing out the mode structure diagnostic. The work of two authors (HLB and JVD) was supported by the U.S. Department of Energy under Contract No. DE-FG05-80ET-53088.

REFERENCES

[1]C. Z. Cheng *et al.*, in *Proceedings of the 15th Conference on Plasma Physics and Controlled Nuclear Fusion Research* (Seville, Spain, 1994), to be published by the IAEA.

[2]E. Fredrickson, in *Proceedings of the 15th Conference on Plasma Physics and Controlled Nuclear Fusion Research* (Seville, Spain, 1994), to be published by the IAEA.

[3]L. Chen, in *Theory of Fusion Plasmas*, ed. J. Vaclavik, F. Troyon, and E. Sindoni (Societa Italiana di Fisica/Editrice Compositori, Bologna, 1989), p. 327.

[4]G. Y. Fu and C. Z. Cheng, Phys. Fluids B **2**, 985 (1990).

[5]F. Zonca and L. Chen, Phys. Fluids B **5**, 3668 (1993).

[6]G. Y. Fu, "Existence of Core Localized Mode," to be published in Phys. Plasmas.

[7]S. Poedts, W. Kerner, J. P. Goedbloed, B. Keegan, G. T. A. Huysmans, and E. Schwarz, Plasma Phys. Contr. Fusion **34**, 1397 (1992).

[8]R. R. Mett and S. M. Mahajan, Phys. Fluids B **4**, 2885 (1992).

[9]J. Candy and M. N. Rosenbluth, Phys. Plasmas **1**, 356 (1994).

[10]H. L. Berk, R. R. Mett, and D. M. Lindberg, Phys. Fluids B **5**, 3969 (1993).

[11]M. N. Rosenbluth, H. L. Berk, J. W. Van Dam, and D. M. Lindberg, Phys. Fluids B **4**, 2189 (1992).

[12]H. L. Berk, J. W. Van Dam, Z. Guo, and D. M. Lindberg, Phys. Fluids B **4**, 1806 (1992).

[13]B. N. Breizman and S. Sharapov, submitted to Phys. Plasmas (IFS Report #671).

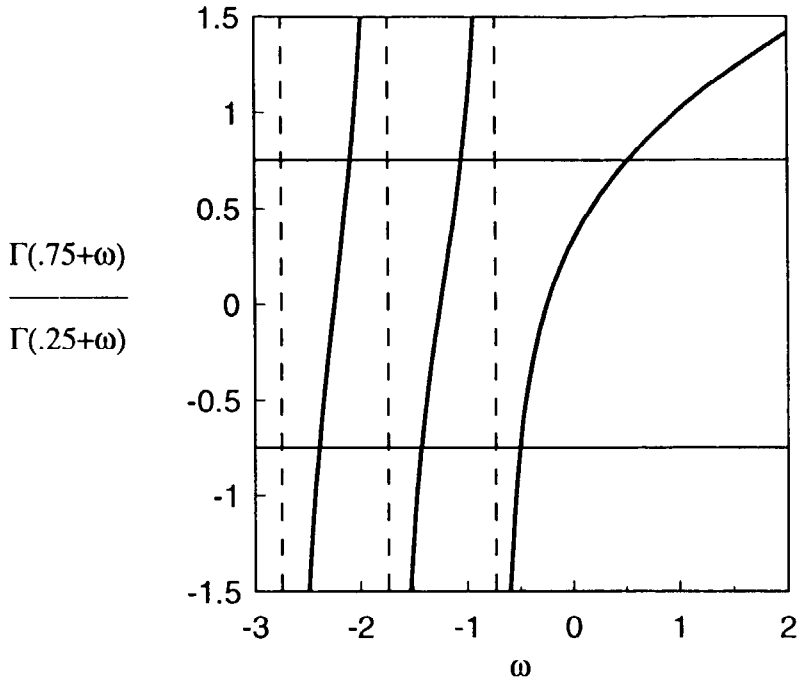

FIG. 1. Graphical plot of the dispersion relation of Eq. (13). Roots occur at the intersections of the curves with the horizontal line that corresponds to the value of a; two cases are shown, one for negative a and one for positive a.

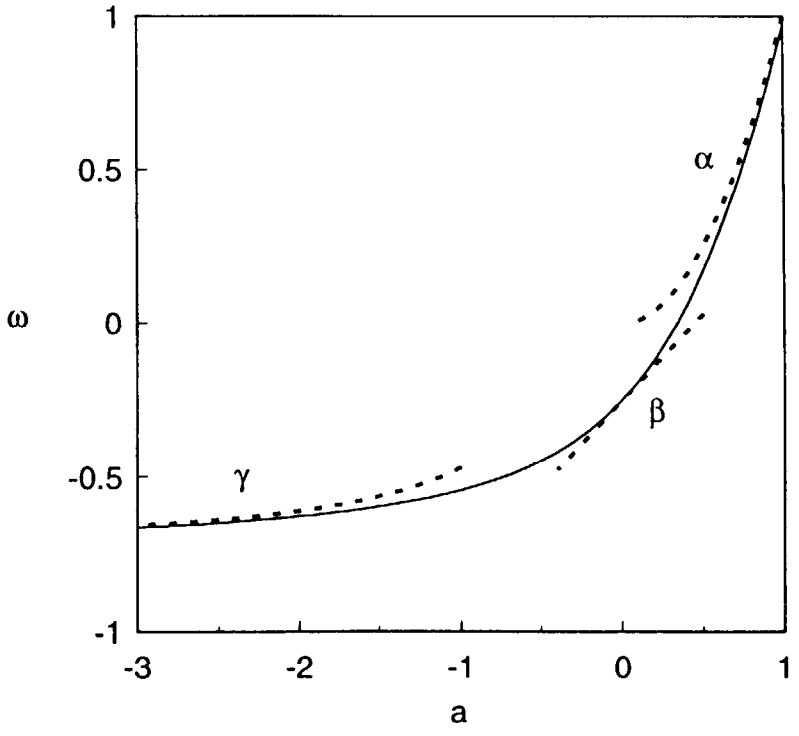

FIG. 2. Eigenfrequency shift $\hat{\omega}$ (solid curve) as a function of the quantity a of Eq. (13), compared to approximate analytic expressions (dashed curves α, β, and γ) for various ranges of a: the ideal TAE limit corresponds to $a^2 \gg 1$.

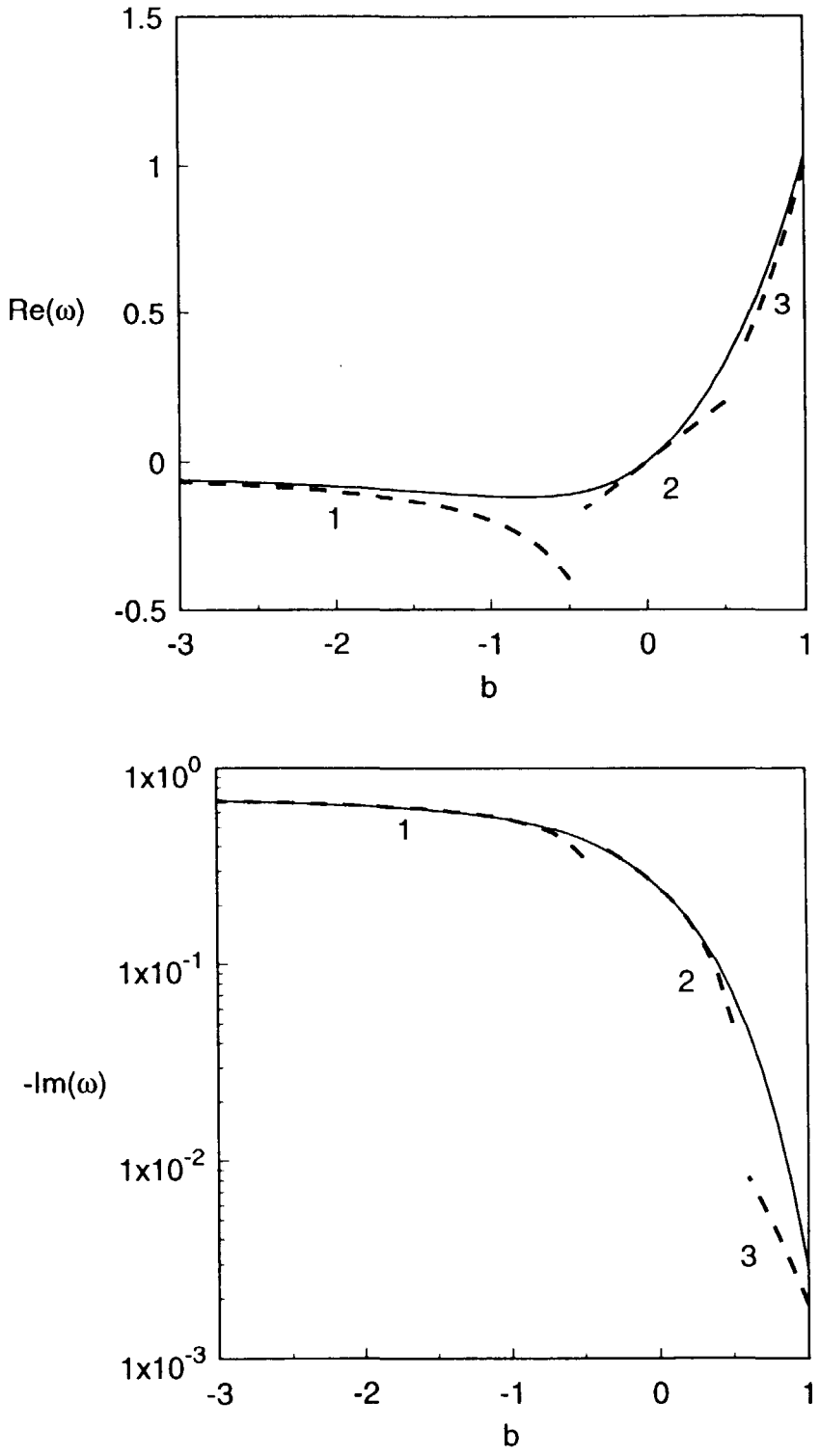

FIG. 3. Complex eigenfrequency shift $\hat{\omega}$ (solid curve) as a function of the quantity b of Eq. (14), compared to approximate analytic expressions (dashed curves 1, 2, and 3) for various ranges of b: (a) $\mathrm{Re}\,\hat{\omega}$; (b) $\mathrm{Im}\,\hat{\omega}$.

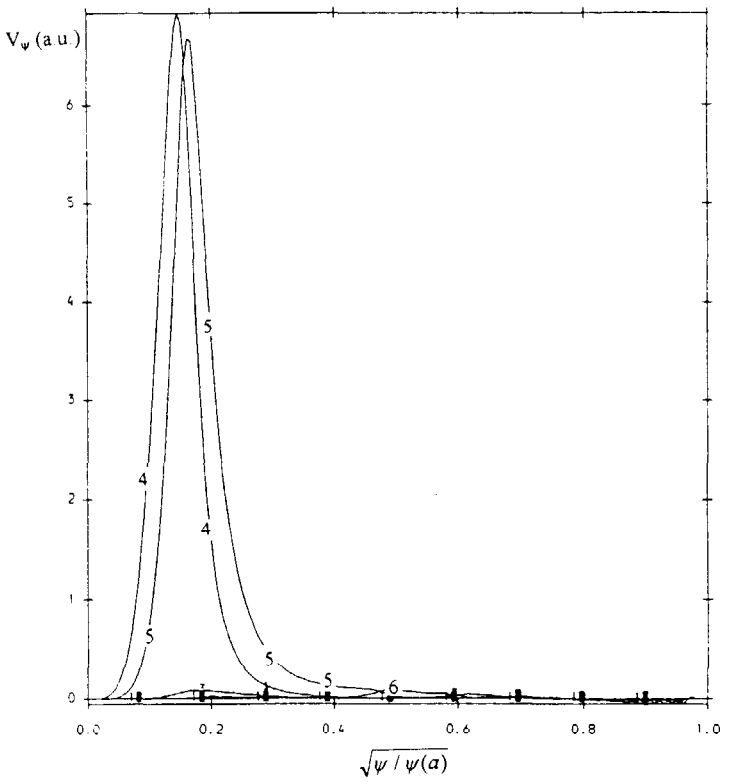

FIG. 4. Eigenfunction of the lower core-localized TAE, calculated from the CASTOR code: $n = 5$ with dominant poloidal harmonics $m = 4$ and 5; eigenfrequency $\omega = 0.5570\, v_A(0)/R_0$.

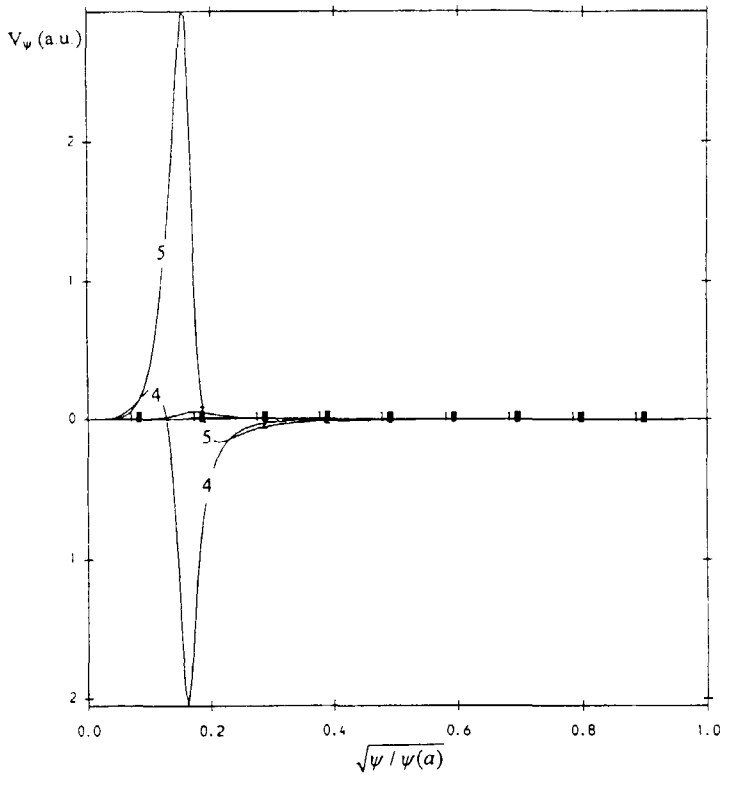

FIG. 5. Eigenfunction of the upper core-localized TAE, calculated from the CASTOR code: $n = 5$ with dominant poloidal harmonics $m = 4$ and 5; eigenfrequency $\omega = 0.5951\, v_A(0)/R$.

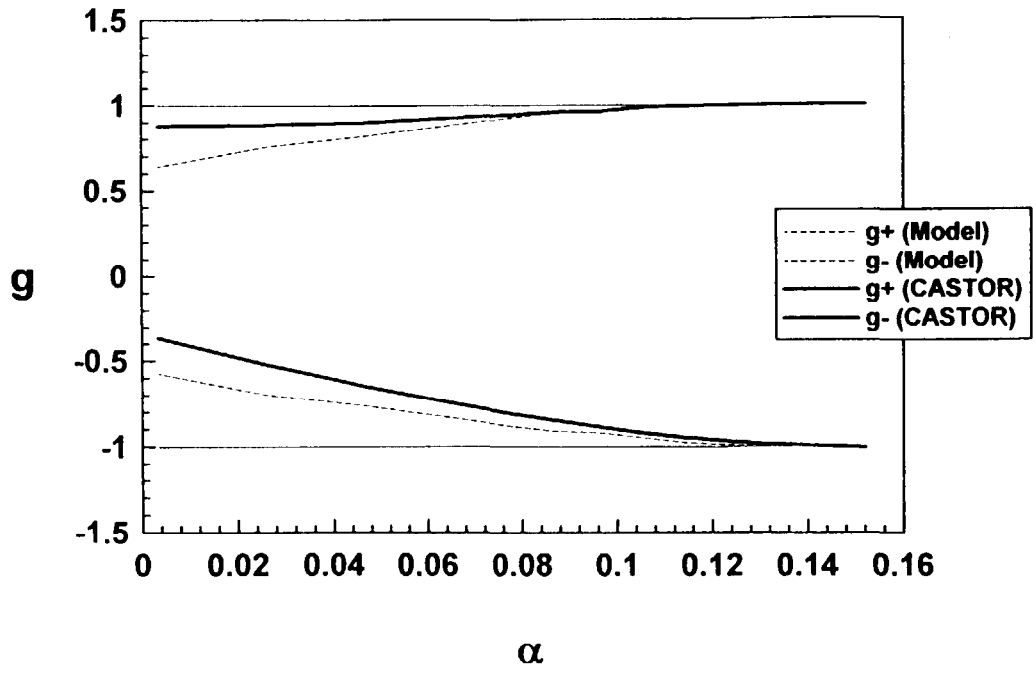

FIG. 6. Upper and lower core-localized TAE eigenfrequencies as calculated from the CASTOR code (thin solid curves) and from integration of the model equations (dashed curves), compared with the CASTOR-calculated upper and lower Alfvén continua (thick solid curves), as functions of the plasma pressure gradient α.

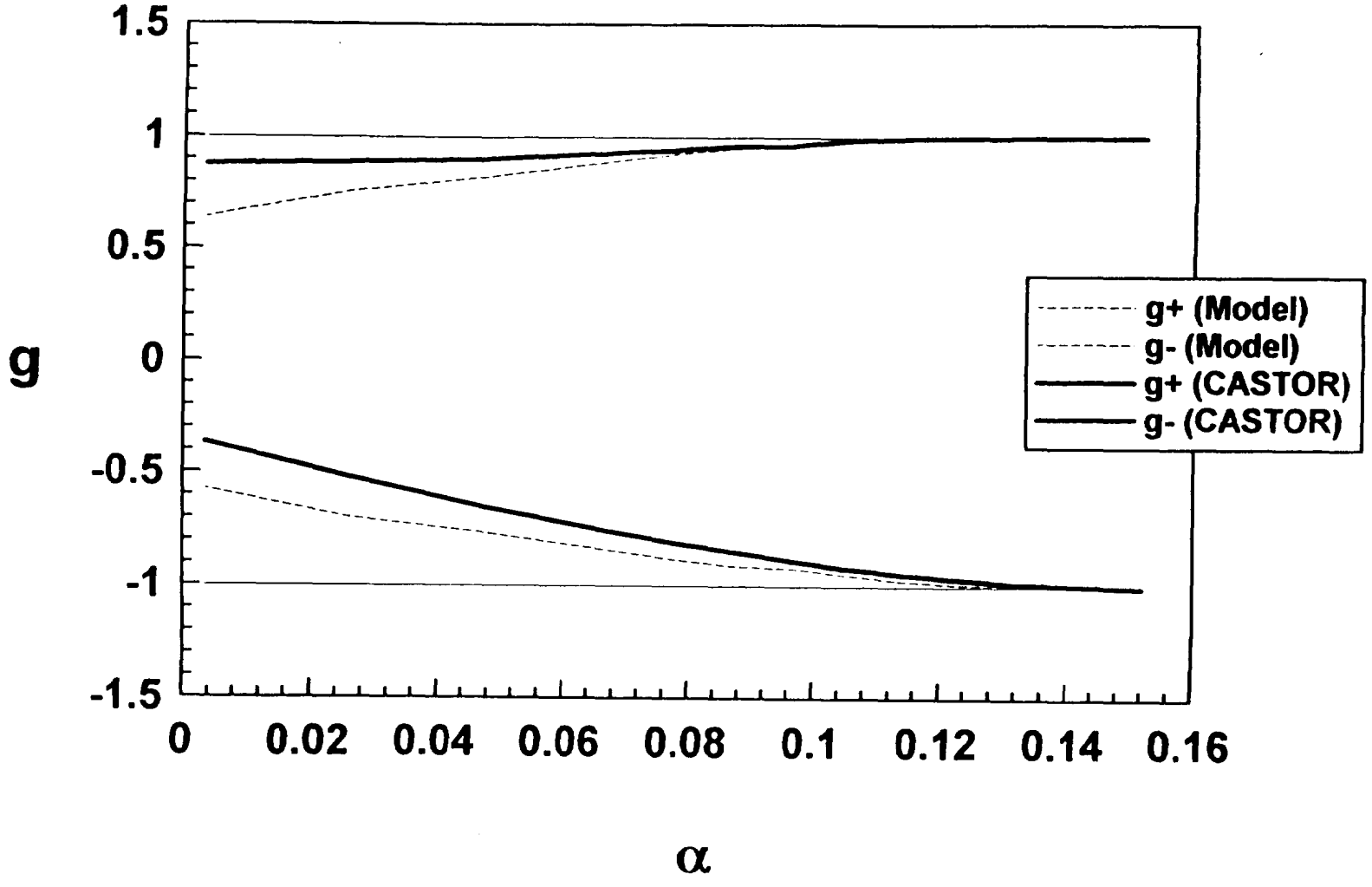
1.5
1
0.5
0
-0.5
-1
-1.5
g
0
0.02
0.04
0.06
0.08
0.1
0.12
0.14
0.16
α
g+ (Model)
g- (Model)
g+ (CASTOR)
g- (CASTOR)

Fig. 6

with the same gap near the center of the plasma, with $\epsilon = 0.035$ and $s = 0.048$. Figure 4 shows the low-end mode, and Fig. 5 the high-end mode, both dominantly consisting of the $m = 4$ and $m = 5$ poloidal harmonics. Note that these modes have opposite polarizations, i.e., $\mathrm{sgn}(\phi_{m=4}/\phi_{m=5}) = -g_0$, and eigenfrequencies located near the corresponding edges of the gap, in qualitative agreement with the theoretical analysis, even though the $\hat{\epsilon} \ll s$ ordering is not satisfied.

Figure 6 shows the CASTOR code results for the mode eigenfrequencies as the central plasma pressure $p(0)$ is increased, together with the results obtained from direct integration of the model equations, Eqs. (2) and (3). For the model equations, parameters were chosen that map the model Alfvén continua onto the CASTOR continua and yield the same values for the quantities s, ϵ, and Δ' as $p(0)$ varies. Both sets of numerical results show that the upper and lower core-localized modes approach the Alfvén continuum with increasing pressure; this behavior also agrees with the analytic prediction. In the CASTOR results, the upper TAE reaches the continuum at $\alpha^{+}_{\mathrm{crit}} \cong 0.131$ (with $\epsilon = 0.035$, $\Delta' = 0.045$, and $s = 0.048$), before the lower TAE does at $\alpha^{-}_{\mathrm{crit}} \cong 0.152$ (with $\epsilon = 0.034$, $\Delta' = 0.050$, and $s = 0.048$), in agreement with the corresponding analytic thresholds $\alpha^{\pm} = \delta \mp s^2$. The results obtained from integrating the model equations also exhibit the same behavior and agreement at threshold. Below threshold, the frequency shift from the continuum as calculated from analytic theory is somewhat different from that obtained from the CASTOR code; we suspect that the high-n approximation in the analytic theory is a source of this disparity.

In Fu's analysis[6] of finite aspect ratio effects (also with the ordering $\hat{\epsilon} \ll s$), he used a ballooning mode type of treatment, which is valid[11] when $n\epsilon e^{-1/s} \gg 1$; this would then lead to replicating local mode structures at each location where $q(r) = (m + 1/2)/n$, for many m values. However, when the opposite inequality $n\epsilon e^{-1/s} \ll 1$ is satisfied, as in our treatment, then the eigenmode will truly have a single localized structure due to the m and $m + 1$ poloidal harmonics near $q(r) = (m + 1/2)/n$. Nevertheless, the eigenvalues obtained with a

ballooning theory will differ only slightly, because the mode overlap between successive gaps is exponentially small in the low-shear limit.

We again note that the lower frequency core-localized mode, found by Fu,[6] tends to be strongly damped by radiation damping as its frequency approaches the continuum, whereas the new core-localized mode at the high end of the gap has negligible radiation damping. Hence this new mode may be experimentally observable at moderate beta values when the other mode is suppressed by radiation damping.

Finally, we note that there may be a relatively straightforward experimental method for distinguishing the upper core-localized mode from the lower one, if appropriate core plasma diagnostics are used. Since their polarizations are determined (in Case 1) by $\phi_m + g_0\phi_{m+1} \cong 0$, the time-averaged power signal corresponding to the lower core-localized mode will peak on the outboard tokamak midplane, being proportional to $\cos^2(\theta/2)$, whereas that for the upper core-localized mode, proportional to $\sin^2(\theta/2)$, will be peaked on the inboard side of the plasma.

We acknowledge our gratitude to Dr. G. Y. Fu for showing us his results prior to publication and checking the comparison with the NOVA-K results, and to Dr. B. N. Breizman for pointing out the mode structure diagnostic. The work of two authors (HLB and JVD) was supported by the U.S. Department of Energy under Contract No. DE-FG05-80ET-53088.